Macromolecules
ARTICLE

Macromolecules **2009**, *42*, 7031–7041 **7031**
DOI: 10.1021/ma901117s

Oxygen Transport Properties of Thiol−Ene Networks

Luke Kwisnek, Sergei Nazarenko, and Charles E. Hoyle*

School of Polymers and High Performance Materials, The University of Southern Mississippi, Hattiesburg, Mississippi 39406

Received May 22, 2009; Revised Manuscript Received August 1, 2009

ABSTRACT: Oxygen transport characteristics, i.e., permeability, diffusivity, and solubility, have been determined for a variety of photopolymerized thiol−ene networks. Despite the abundance of thiol−ene research and the importance of such information, it is until now absent from the literature. One model network, which showed high oxygen barrier properties, was selected for further modification. Covalent bonding of functional groups to the network was enabled by an interesting approach: thio-Michael addition of various functionalized acrylates to a tetrathiol monomer. Cyano, hydroxyl, amide, and alkyl functional groups were explored. These new modified thiols were subsequently copolymerized with an isocyanurate-based multifunctional ene. This modification technique enabled a study on how different functional groups embedded in a uniform network affect T_g and oxygen barrier properties. All studied networks exhibited oxygen diffusivity and permeability which both spanned nearly 3 orders of magnitude. Correlation of both oxygen permeability and oxygen diffusivity with T_g was observed. This correlation allows the prediction of oxygen barrier properties of thiol−ene networks using T_g.

Introduction

The use of polymers in gas barrier applications is well-documented, especially in the case of oxygen transport.[1−3] Oxygen uptake is of key concern with food, beverage, and other packaging applications.[3] While the polymer must be easily processed and often in high volumes, the key property for selection of such materials is gas permeability. The rate of gas transport through polymer films, while improvable through factors such as orientation, crystallinity, and addition of high-aspect ratio particulates,[4] is primarily determined by the chemical natures of the penetrant and the polymer.[1] Polymers with strong secondary forces obtained through dipole−dipole interactions and hydrogen bonds that lead to tight packing and low free volumes have naturally high barriers to nonpolar gases like oxygen and nitrogen: examples include polyacrylonitrile, poly(styrene-co-acrylonitrile), poly(vinylidene chloride), poly(vinyl alcohol), and some polyamides.[3] Using the functional groups of these high-barrier polymers as models, White devised a plethora of high-barrier thermoplastics based on epoxy chemistry including poly(hydroxyl ether sulfonamides)[5] and poly(hydroxy amide ethers).[6] The common thread among these materials is an enhancement in intermolecular cohesion via the inclusion of amide, sulfone, and hydroxyl groups which subsequently improves the barrier to oxygen.

While the high-barrier field may be well surveyed, improvement of the oxygen barrier of polymers is a perpetual task; recent technologies include new liquid crystalline polymers, multilayered systems and blends, and both organic and inorganic coatings.[3] Coatings are a common solution to barrier problems, and photocurable films offer potentially attractive benefits when used as coatings since they are eco-friendly, generally comprise 100% reactive components, and cure rapidly when exposed to UV-light.[7] With regards to barrier properties of photopolymerized materials, oxygen transport properties of a UV-cured acrylate coating have been reported: Mathias et al. reported barrier improvement of PET beverage bottles coated with a UV-curable liquid methacrylate followed by UV-photopolymerization.[8] In contrast to acrylates, photopolymerized thiol−ene networks gel at high conversion leading to low shrinkage, homogeneous network density, and uniform glass transitions.[9] Thiol−ene photopolymerization also occurs readily in the presence of oxygen. The polymerization of a thiol−ene network follows a free-radical process, not a typical chain-growth reaction, that proceeds via a step-growth free-radical chain mechanism with two propagation steps.[9]

The unprecedented uniformity of thiol−ene networks, coupled with the ability to bind specific functional groups to the network without altering the basic network structure, provides an outstanding opportunity for evaluating structural effects on gas transport properties. In addition, there is a need for assessment of gas transport in thiol−enes. The only published data on barrier properties of UV-cured thiol−ene materials is by Mather and Pintauro: a neat NOA63 film was reported to have an oxygen permeability comparable to PET, indicating potential for thiol−enes in oxygen barrier or membrane applications.[10] And with decades of published oxygen transport research on a multitude of polymeric materials, it is important to note that sulfur-containing polymers and coatings are under-represented even while other coatings like SiO_x are currently used and well-documented.[3] Herein, we report in detail the oxygen transport properties of free-standing thiol−ene films that have strongly interacting functional groups incorporated into the network. The expectation is that such groups, inferable by the work of Salame[1] and White et al.[5,6] in linear polymer systems, when incorporated into a highly uniform network will provide a conclusive description of how the transport properties of highly uniform structured networks can be tuned.

Experimental Section

Materials. Thiol monomers trimethylolpropane tris(3-mercaptopropionate) (3T) and pentaerythritol tetrakis(3-mercaptopropionate) (4T) were supplied by Bruno Bock Thiol-Chemical-S; thiol monomer tris[2-(3-mercaptopropionyloxy)ethyl] isocyanurate (3TI) was obtained from Yodo Chemical Co. Ltd. Ene monomers

*Corresponding author. E-mail: Charles.Hoyle@usm.edu.

Published on Web 08/21/2009

Chart 1. Thiols, Enes, and Isocyanate

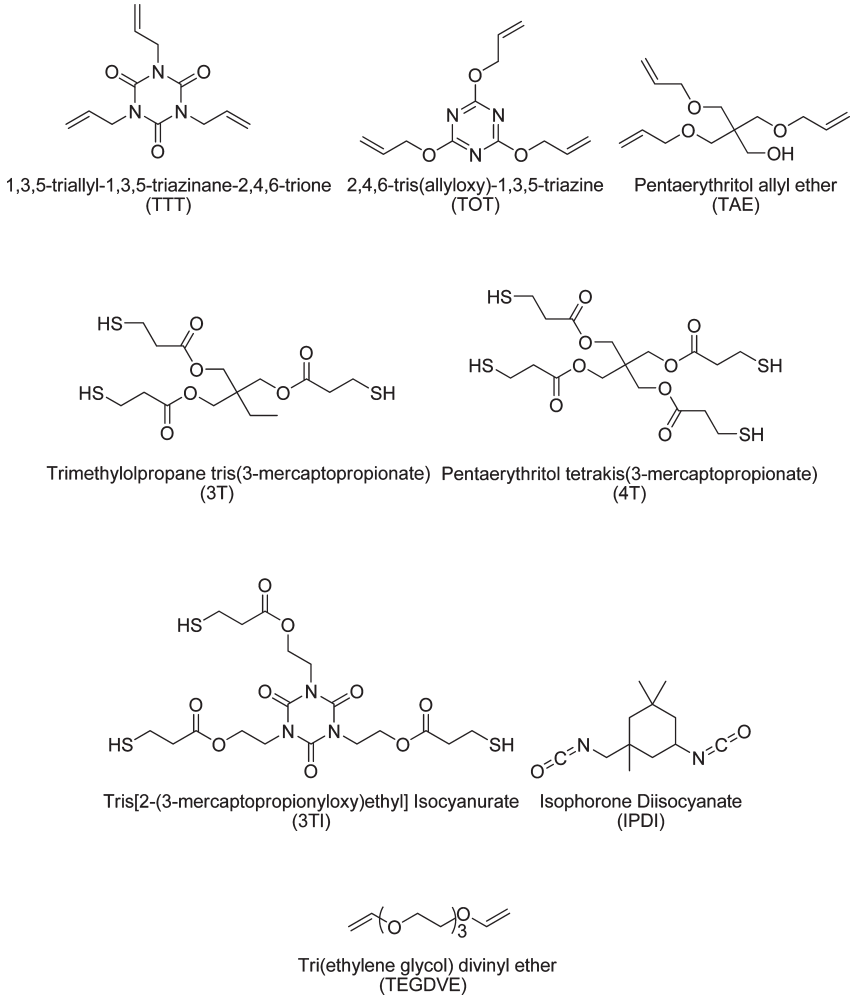

tri(ethylene glycol) divinyl ether (TEGDVE), pentaerythritol allyl ether (TAE), and 2,4,6-triallyloxy-1,3,5-triazine (TOT) were obtained from Aldrich. Ene monomer triallyl-1,3,5-triazine-2,4,6(1*H*,3*H*,5*H*)-trione (TTT) was supplied by Sartomer. Thiol and ene structures are shown in Chart 1. Ethyl acrylate (EA), acrylamide (Am), acrylonitrile (AN), 2-hydroxyethyl acrylate (HEA), *N*-isopropylacrylamide (NIPAM), diethylamine, and tributylamine were obtained from Aldrich (see Chart 2). Isophorone diisocyanate (IPDI) was provided by Bayer Material Science. The cleavage-type photoinitiator α,α-dimethoxy-α-phenylacetophenone (Irgacure 651) was supplied by Ciba Specialty Chemicals. Acetone-d_6, obtained from Aldrich, was used to conduct NMR measurements. All chemicals were used as received.

Synthesis of Modified Thiol Monomers. Modified trifunctional thiol monomer mixtures were synthesized using an amine-catalyzed thio-Michael addition reaction between 4T and EA, Am, AN, HEA, and NIPAM at a 1:1 molar ratio so as to cap an average of one of the four thiol groups. Synthesis of products 4T-EA, 4T-AN, and 4T-HEA was accomplished by first adding a quantity of 4T and 1 wt % diethylamine to a round-bottom flask. An equal molar quantity of the appropriate small molecule was then weighed in a separate vial and then added dropwise to the 4T/catalyst mixture at ~1 mL/min while stirring. The flask was then sealed and allowed to stir overnight. Syntheses of products 4T-Am and 4T-NIPAM require that acrylamide and *N*-isopropylacrylamide first be dissolved in acetone and then added dropwise at 1 mL/min while stirring. The flask was then sealed and allowed to stir overnight, at which point the mixture is placed in a rotovap at 60 °C for 2 h to remove acetone and leave either a 4T-Am or 4T-NIPAM liquid product. A third procedure was used to synthesized 4T-Am:EA monomer mixtures. First, 4T and 1 wt % diethylamine were mixed in a round-bottom flask. Am and EA at appropriate molar ratios were combined and dissolved in acetone. This mixture was then added dropwise to the 4T/catalyst mixture at 1 mL/min while stirring and the reaction was allowed to proceed overnight. These mixtures are rotovapped for 2 h at 60 °C as above to remove acetone. The final monomers are a distribution of structures with the trifunctional monomer being predominant. It is noted that the distribution could result in small changes in the macroscopic physical properties of the final networks versus networks formed from a purely trifunctional system.

Chart 2. Small Molecules and Amine Catalysts

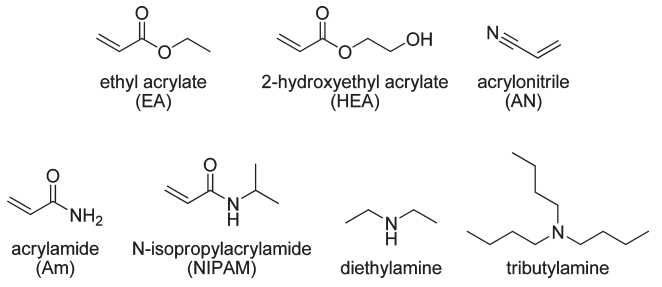

Characterization of Products and Polymerization Kinetics. Modified thiol monomer products were characterized by ^{1}H NMR using a Varian Mercury 200 MHz NMR spectrometer in

acetone-d_6. Polymerization kinetics of selected control films and modified thiol−ene films were monitored using a Bruker 88 FTIR spectrometer modified with a fiber-optic cable to irradiate samples sandwiched between two salt plates. The conversion of thiol −SH groups at 2570 cm^{-1} (S−H stretch) and ene C=C groups at 3100 cm^{-1} (vinyl C−H stretch) were monitored as a function of irradiation time. An Oriel 200 W high-pressure mercury−xenon lamp with light intensity of 6.16 mW/cm^2 at 365 nm was used to irradiate the samples and invoke photopolymerization.

Film Formation. Free-standing thin films of all thiol−ene formulations were made by dissolving 1 wt % 1,1-dimethoxy-1-phenylacetophenone (Irgacure 651) photoinitiator into the thiol−ene mixture by sonication for ~10 min. This homogeneous mixture was then drawn down onto glass substrates using drawdown bars. Initial scouting work determined optimal thickness: materials with oxygen permeability less than 0.2 cm^3 (STP) cm m^{-2} day^{-1} atm^{-1} were cast using a 0.13 mm drawdown bar while those with higher permeability were drawn down anywhere from 0.51 to 1.3 mm thickness depending on the permeability value. This procedure was done to ensure an adequate amount of experimental data points in the non-steady-state region of the flux curves for proper fitting. Films were cured using 10 passes under a Fusion UV curing line system with a D bulb (400 W/cm^2 with belt speed of 3 m/min and 3.1 W/cm^2 irradiance). All films were normalized in air for 3−5 days prior to testing. Annealing of films was investigated using an annealing procedure of 100 °C for 4 h in air—this was done to verify if the UV-curing process was sufficient for full conversion of films and to complement the oxygen permeation results for unannealed films to show reproducibility.

Oxygen Permeation Testing. Oxygen permeation tests were conducted on Mocon OX-TRAN 2/21 instruments using a continuous-flow testing cell method approved by the ASTM (D3985). All measurements were conducted at 23 °C and 0% RH. In this method, oxygen is the test gas and inert nitrogen is the carrier gas. The samples of 50 cm^2 testing area were loaded into the testing cell and flushed with nitrogen gas to purge out excess gases and to develop a zero point. Afterward, pure oxygen gas was introduced to one side of the test cell; the driving force for permeation is a difference in partial pressure of oxygen since the concentration of oxygen on the carrier side of the cell is maintained at essentially zero. Oxygen was carried away from the downstream surface of the film by the nitrogen carrier gas to a coulometric sensor.

Permeability P and diffusivity D were obtained by performing a two-parameter least-squares fit of the experimental oxygen flux $J(t)$ data to Fick's second law solution (eq 1):[11]

$$J(t) = \frac{Pp}{l}\left[-\sum_{n=1}^{\infty}(-1)^n \exp(-D\pi^2 n^2 t/l^2)\right] \quad (1)$$

where p is the applied pressure and l is the film thickness. Using the solution-diffusion equation (eq 2),[12] the solubility S was then calculated.

$$P = DS \quad (2)$$

Instrumentation error using this method in the range of oxygen fluxes studied is ±5% for permeability values and ±10% for diffusivity values. The remaining experimental error in obtaining P, D, and S values is largely derived from film thickness variations. For this reason, special care was taken to evaluate films of approximately uniform thickness; thickness averages were obtained by measuring at multiple locations.

Thermal and Mechanical Analysis. A TA Instruments Q1000 DSC with heating rate of 10 °C/min was used to investigate the glass transition temperature of film samples between 8 and 12 mg. Mechanical properties were evaluated using a Rheometric Scientific DMTA V with a frequency of 1 Hz, strain rate of 0.05%, and heating rate of 5 °C/min. T_g values were taken as the midpoint of the inflection from DSC scans and as the peak maximum in tan delta plots from DMTA.

Results and Discussion

Basic Thiol−Ene Networks. In order to establish a baseline in properties, the oxygen transport characteristics of basic thiol−ene films were evaluated. These basic networks feature the 3T trifunctional thiol monomer copolymerized with four different ene monomers of varying functionality and rigidity: TEGDVE, TAE, TOT, TTT. TEGDVE, the least rigid monomer, is difunctional, while TAE, also a flexible monomer, is trifunctional. TOT and TTT have basic triazine and isocyanurate structures and are more rigid trifuctional ene monomers. The trifunctional thiol 3TI and tetrafunctional 4T were also copolymerized with TTT to increase the network rigidity and the glass transition temperature. All thiol−ene networks were obtained by exposing 1:1 molar functional group mixtures with 1 wt % photoinitiator to 10 passes under a medium pressure D bulb as detailed in the Experimental Section. A high-T_g thiol−isocyanate−ene film for comparison was prepared from a one-pot mixture of 6 mmol of 4T, 4 mmol of IPDI, 5.3 mmol of TTT, 1 wt % Irgacure 651, and 0.05 wt % tributylamine. The liquid mixture was drawn down and cured in the same fashion as the basic thiol−enes. A portion of thiols reacted with the isocyanates via the tributylamine catalyst, and the remaining thiols reacted with the TTT enes via photopolymerization. This film was then postcured for 12 h at 110 °C; the result is a high-T_g cross-linked network with carbamate groups present that enhance hydrogen bonding. Note that this three-component film was not considered a basic thiol−ene film and was included only for comparison as a high-T_g, highly cross-linked network.

Figure 1 shows DSC second heating scans for each of the resulting thiol−ene networks. T_g values are listed in Table 1. As has been reported for photocured thiol−ene networks,[8,9] the DSC curves exhibit well-defined, narrow glass transition regions indicative of their high uniformity. It is important to note that simply by changing the ene component the glass transition temperature of the film changes dramatically; this series of six thiol−ene films spans over 80 °C in glass transition temperatures. The T_g values are directly related to the thiol and ene functionalities as well as their rigidity as detailed in refs 14−16. The 4T-IPDI-TTT film has a T_g of 65 °C, which is well above room temperature, thus making it a decidedly glassy network for the oxygen transport measurement.

Oxygen transport measurements of the basic thiol−ene films were next conducted using a continuous-flow testing

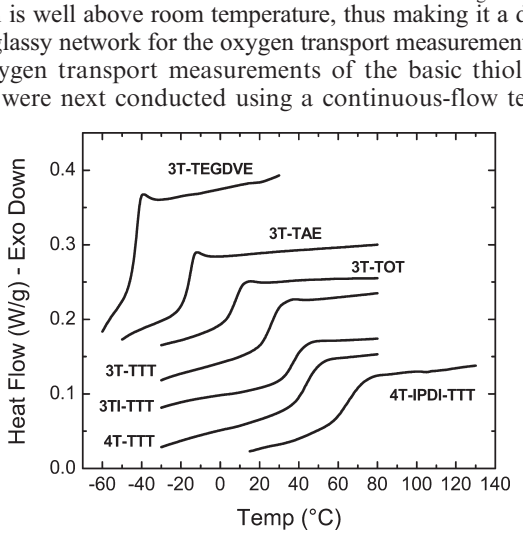

Figure 1. DSC second heating scans for basic thiol−ene films and thiol−isocyanate−ene film.

Table 2. Oxygen Transport Data for Thiol−Ene Networks and PET for Comparison

	oxygen permeability (cm^3 (STP) cm m^{-2} day^{-1} atm^{-1})			
material	normal	annealed	oxygen diffusivity (cm^2 s^{-1})	oxygen solubility (cm^3 (STP) cm^{-3} atm^{-1})
3T-TEGDVE	13.8		3.4×10^{-7}	0.047
3T-APE	1.6		4.2×10^{-8}	0.044
3T-TOT	0.22		6.6×10^{-9}	0.038
3T-TTT	0.090	0.10	4.0×10^{-9}	0.027
4T-TTT (1:1)	0.032	0.032	1.4×10^{-9}	0.027
4T-TTT (4:3)	0.041	0.042	1.7×10^{-9}	0.026
3TI-TTT	0.021	0.024	1.0×10^{-9}	0.025
4T-IPDI-TTT	0.12		4.2×10^{-9}	0.034
4T-EA-TTT	0.39	0.45	2.4×10^{-8}	0.019
4T-AN-TTT	0.090		6.0×10^{-9}	0.017
4T-HEA-TTT	0.16	0.16	4.5×10^{-9}	0.041
4T-NIPAM-TTT	0.19		5.8×10^{-9}	0.038
4T-Am-TTT	0.030	0.030	2.2×10^{-9}	0.015
25:75 Am:EA	0.22		6.5×10^{-9}	0.039
50:50 Am:EA	0.11		4.5×10^{-9}	0.028
75:25 Am:EA	0.076		4.2×10^{-9}	0.021
PET	0.36		5.0×10^{-9}	0.083

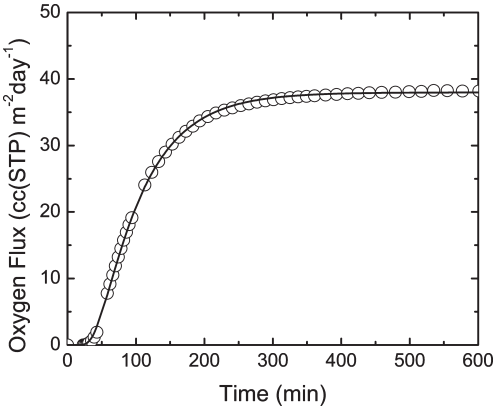

Figure 2. Representative oxygen flux fit curve for 3T-TAE film of 0.42 mm thickness.

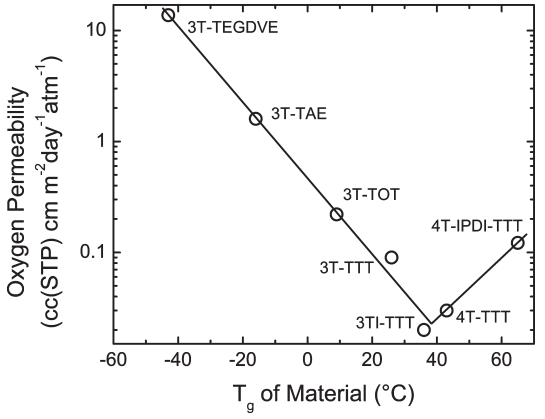

Figure 3. Relationship between oxygen permeability and the T_g of basic thiol−ene materials.

system described in the Experimental Section. Figure 2 shows a representative experimental oxygen flux data (opened symbols) obtained at room temperature for a 3T-TAE film of 0.42 mm thickness with the two-parameter fit to eq 1 (solid line). The fit was excellent. The experimental oxygen flux curves for all samples exhibited the same type of Fickian behavior shown in Figure 2. Equation 1 was used to fit flux data and calculate permeability (P) and diffusivity (D). Using eq 2, the solubility (S) was calculated. The

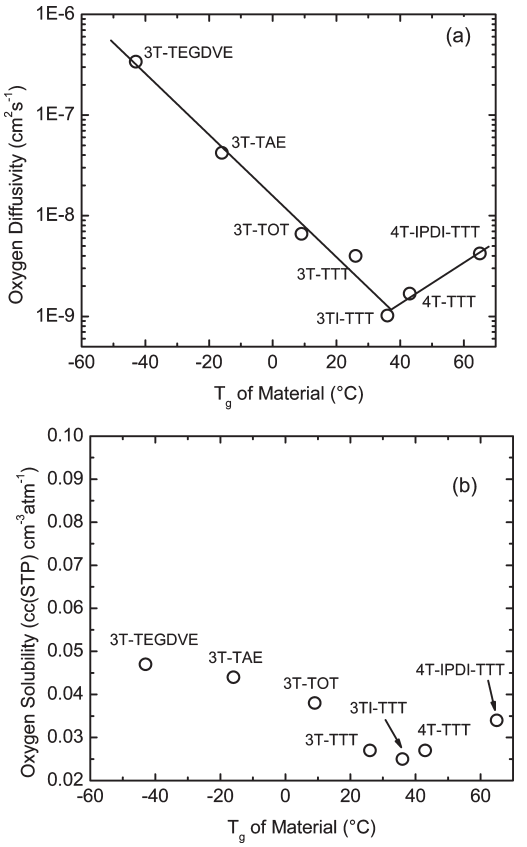

Figure 4. Relationship between (a) oxygen diffusivity and T_g and (b) oxygen solubility and T_g of basic thiol−ene materials.

individual P, D, and S values of the six basic, two-component thiol−ene films are given in Table 2. These data are also plotted as a function of T_g in Figures 3 and 4.

For rubbery networks exhibiting glass transition temperatures below room temperature, the temperature (23 °C) at which all transport measurements were conducted, P and D exponentially decreased as T_g increased. In turn for glassy networks exhibiting T_g above room temperature, in particular for 4T-TTT and 4T-IPDI-TTT, P and D exponentially increased with T_g. A minimum in both oxygen permeability and diffusivity is thus observed near the testing temperature. These two dependencies in semilog coordinates displayed an

almost perfect V-shape trend as one can see in Figures 3 and 4a.

The V-shape trend of P, D, and S with T_g has been interpreted in this article by means of a free volume concept broadly used in the literature to interpret gas barrier data. It is widely accepted that P, D, and S of a polymer increase with the free volume. While solubility changes somewhat in proportion to the amount of free volume, diffusivity and subsequently permeability exhibit an exponential dependence on free volume.[17]

In general, *rubbery* polymers exhibit a correlation between free volume and the difference between T_g and T_{test} (T_{test} is the temperature at which the measurement was made). The results of free volume and gas transport measurements conducted at a specific T_{test} on different polymers with a broad range of T_g are as follows. Beginning with the lowest T_g polymer and advancing to polymers of higher T_g, the difference between T_g and T_{test} decreases, and both the free volume and gas diffusivity are reduced.[18,19] Once the T_g of the material surpasses T_{test}, the polymer is in the glassy state during the measurement. For *glassy* polymers with increasing T_g the free volume and gas diffusion coefficient at T_{test} both increase[18] since transport is enhanced by the presence of hole-free volume that is frozen into the glassy, nonequilibrium state.[20] It is noted that such static hole-free volumes do not exist in the rubbery state.[20] As the difference between T_g and T_{test} increases for glasses, the amount of frozen hole-free volume also increases. In summary, there is a clear minimum for both free volume and gas diffusivity where $T_{test} = T_g$. This is precisely the result seen with the basic thiol−enes when combining the results for both rubbery and glassy networks: exponential dependencies of permeability and diffusivity vs T_g, with minimums near T_{test}.

As expected, oxygen solubility for thiol−enes in Figure 4b also shows a minimum. Similar behavior was shown for the relationship between oxygen solubility and the T_g for PET—a minimum in oxygen solubility appears at $T_{test} = T_g$.[11] The TTT-based films in particular display low oxygen solubility; in fact, solubility that is almost 3 times lower than PET. This results from the scarcity of free volume in the highly dense cross-linked thiol−ene networks as compared to linear, amorpohous PET[13] which is glassy at room temperature. As well, the sulfur present in the networks may also contribute to the low solubility of oxygen.

It can be concluded that the basic thiol−enes, while having different T_g, different functionalities, different ene groups, and different monomer rigidities, belong to the same *family* in terms of oxygen transport properties. The permeability and diffusivity values correlate well with the difference between T_g and T_{test} and form a minimum, allowing prediction of these characteristics from this semilog relationship. While these results are consistent with well-known observations, they represent to the best of our knowledge the first report of the correlation of T_g and transport properties for a family of highly cross-linked thiol−ene networks that obeys a prototypical fit.

Modified Thiol−Ene Networks. Having established benchmark oxygen transport properties for commercially available thiol and ene monomers, the tunability of the thiol−ene networks was explored. In the past, the effect of a plethora of functional groups and repeat units on the gas barrier properties of linear polymers has been evaluated phenomenologically.[1,2] The three most effective structural units for decreasing oxygen permeability were the cyano group, the hydroxyl group, and the amide repeat unit. The primary amine catalyzed thiol−acrylate Michael addition reaction in Figure 5 was used to develop a platform to assess the effect of a wide range of functional groups including alkyl, hydroxyl, cyano, primary amides, and secondary amides on T_g and oxygen barrier properties.

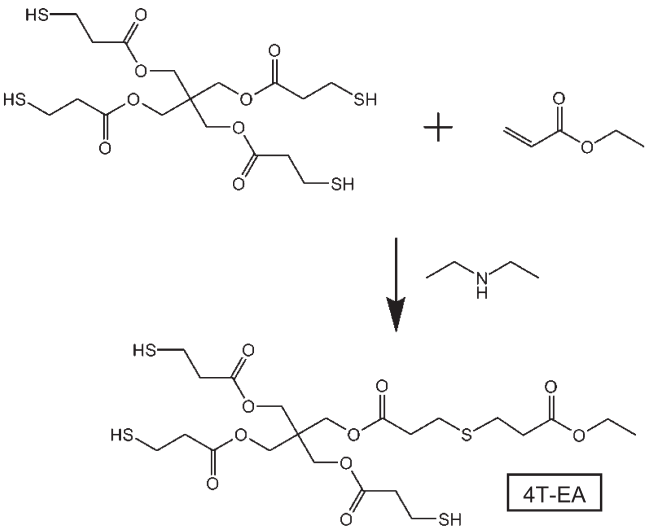

Figure 5. Thio-Michael addition reaction mechanism of 4T and EA with diethylamine catalyst. Product shown is representative of predominant structure in the mixture. Other products were formed by reacting 4T with the other enes in Chart 2 (i.e., 4T-AN, 4T-HEA, 4T-NIPAM, and 4T-AM).

In order to verify that all of the respective electron deficient ene effectively reacted via the thiol−acrylate Michael reaction, each of the products were characterized by ^{1}H NMR. Figure 6 shows ^{1}H NMR spectra of the precursor 4T and products 4T-EA, 4T-AN, 4T-HEA, 4T-NIPAM, and 4T-Am. The near-complete loss of the double-bond protons at ~6 ppm indicated that the thiol−acrylate Michael reaction was successful.

The modified trifunctional thiol monomers were photopolymerized with the TTT ene monomer to form a set of thiol−ene networks for systematic evaluation of chemical structural effects on D and S. Results can be readily compared with the 4T-TTT (4:3) network with a *dangling* thiol group, the 3T-TTT network, and the 4T-EA-TTT network which has a nonpolar ethyl group that is also incapable of hydrogen bonding. This series of films serves as a convenient model for establishing the effect of different dangling functional groups on D and S in a highly uniform cross-linked network. The thiol−ene system is in general well-suited for such a study because it is highly uniform, it is characterized by high functional group conversions, it has no crystallinity, and the molecular weight variation between cross-links is essentially identical for all of the systems investigated. How a particular functional group incorporated into a uniform network affects glass transition temperature and oxygen transport properties will be realized.

Real-time IR photopolymerization kinetics for the modified thiol−ene systems are shown in Figure 7. The thiol and ene functional groups proceed rapidly to high conversion at room temperature. The 4T-EA-TTT and 4T-HEA-TTT systems attained the highest conversion, i.e., 90% for both the thiol and ene functional groups. The 4T-AN-TTT system and 4T-NIPAM-TTT systems reached approximately 80% and 85% conversion, respectively, under the polymerization conditions used. Lastly, the 4T-Am-TTT system reached the lowest conversions of 75%. The thiol and ene conversions in all cases are essentially identical, indicating that the free-radical thiol−ene reaction proceeds rapidly with no indication of ene homopolymerization. This conformity also reinforces ^{1}H NMR results that the 4T-modified monomers

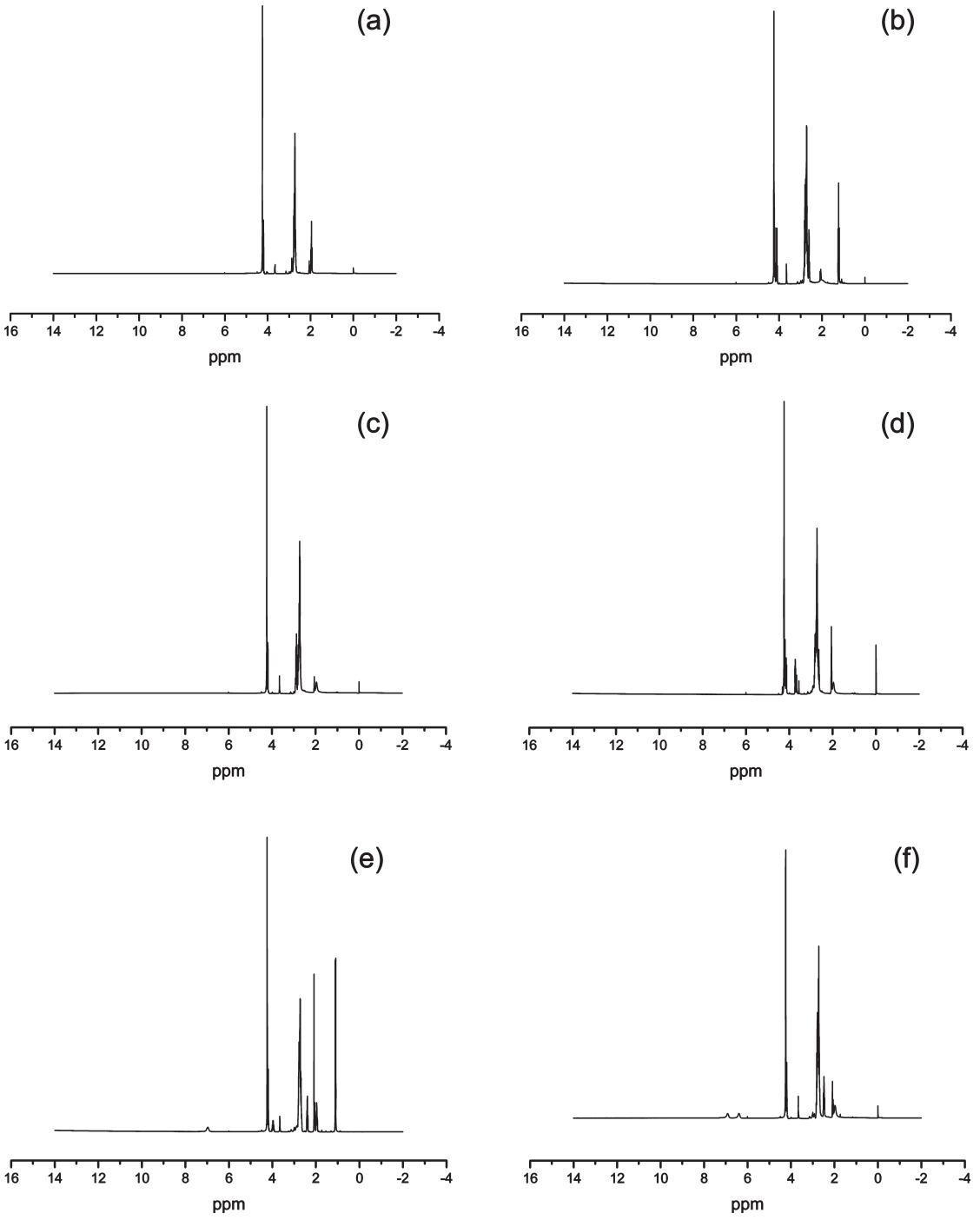

Figure 6. ^{1}H NMR spectra for (a) 4T, (b) 4T-EA, (c) 4T-AN, (d) 4T-HEA, (e) 4T-NIPAM, and (f) 4T-Am.

are stoichiometrically trifunctional on average. Note that the light intensity used in monitoring these polymerization kinetics is smaller than that of the light used to cure films for evaluation where conversions reach nearly 100%.

IR measurements at various temperatures were conducted to verify the presence of hydrogen bonding in the O−H stretching region of 4T-HEA-TTT in accordance with prior IR temperature measurements on poly(HEA).[21] A liquid mixture of 4T-HEA, TTT, and 1 wt % Irgacure 651 was sandwiched between two salt plates and compressed to form a thin layer followed by photopolymerization using the procedure described previously. Spectra were recorded at 23 (room temperature), 60, 100, 140, and 180 °C. As Figure 8 shows, as temperature increased the spectrum shifts to higher wavenumbers, the associated proton shoulder/peak at ~3450 cm^{-1} decreases in intensity, and the entire O−H stretching region decreases in intensity. This is in agreement with results on poly(HEA) films when subjected to higher temperatures and indicates that both associated and free protons are present at room temperature, with reduction in the associated protons with increasing temperature.[21]

The second DSC heating scans for all the cured networks in Figure 9a have narrow glass transitions which are characteristic of thiol−ene films and indicate highly uniform networks. In each case, the networks containing the hydroxyl, primary and secondary amides, and cyano groups show an increase in T_g when compared to the 4T-EA-TTT-based

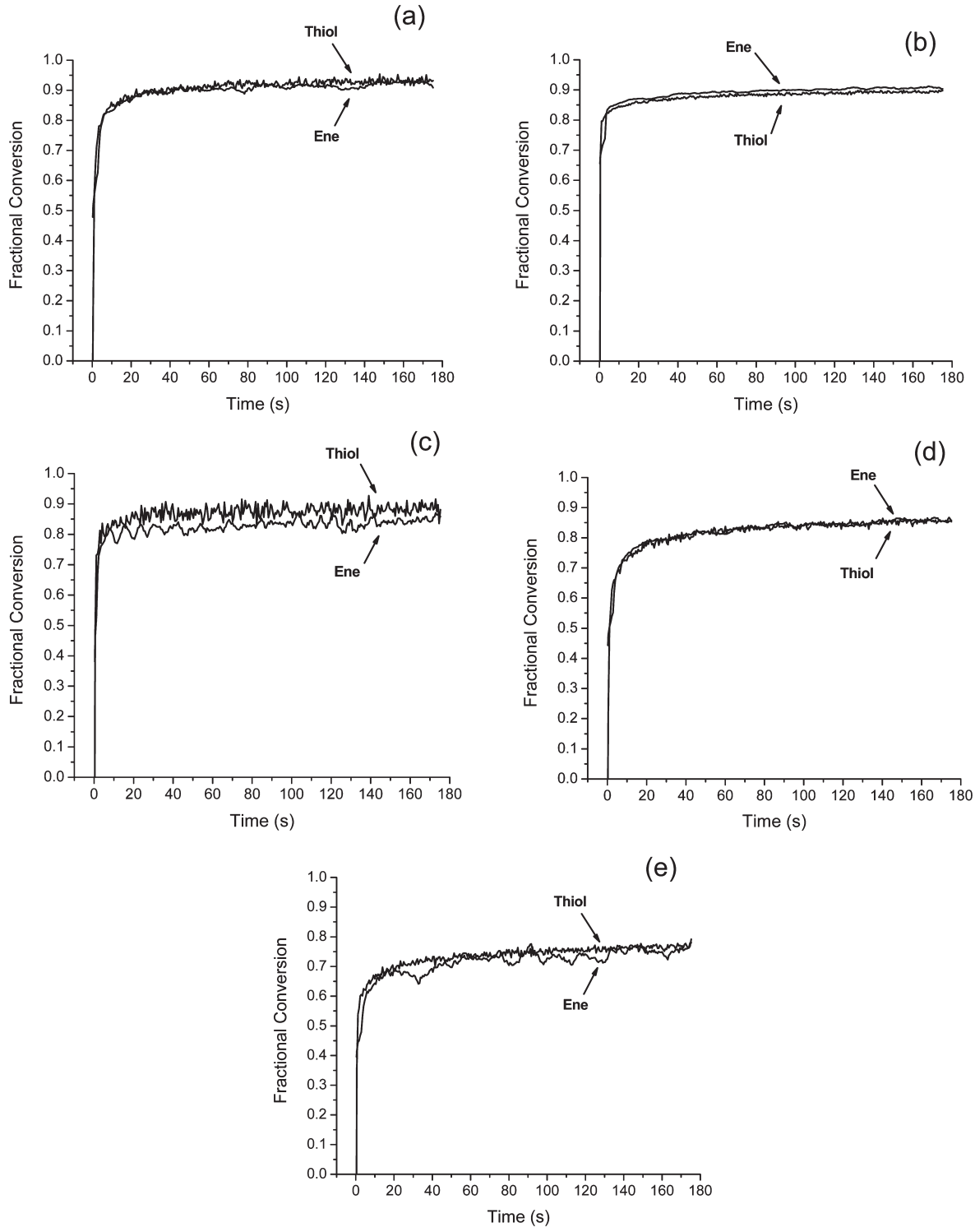

Figure 7. RT:FTIR conversion versus time plots for (a) 4T-EA-TTT, (b) 4T-HEA-TTT, (c) 4T-NIPAM-TTT, (d) 4T-AN-TTT, and (e) 4T-Am-TTT.

network, which only has a hydrocarbon side group with no possibility for polar interaction or hydrogen bonding. This suggests that in each case either dipole−dipole or hydrogen-bonding interactions result in an increase in the glass transition temperature and rigidity of the film. The 3T-TTT control film has a T_g equal to or higher than any of the modified films presumably due to the absence of any *dangling* side groups attached to the network. A free thiol group in the network of the 4T-TTT(4:3) film results in a glass transition between that of the 3T-TTT and 4T-TTT(1:1) films. This clearly shows that a free thiol-functional arm in the network increases the glass transition of the film compared to any of the modified thiol−ene films. This may well be due to a chemical-based structural effect or to the distribution of thiol functional species that actually comprise the modified trifunctional thiols, i.e., the thiol functionality for the 4T-modified systems only represents a nominal average functionality. In order to further evaluate the thiol−ene networks, DMTA measurements were made on each film. As seen in Figure 9b, the basic trends for the peak maximum in the tan delta versus temperature plots are essentially the same except that in each case the

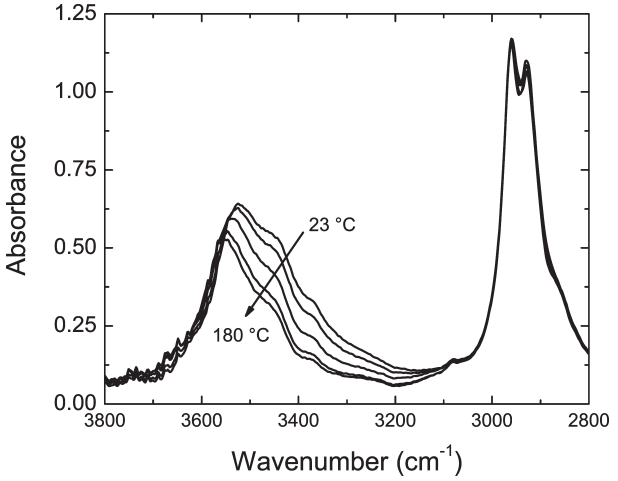

Figure 8. Effect of temperature on IR spectra of 4T-HEA-TTT film in the O−H stretching region demonstrating the presence of hydrogen bonding.

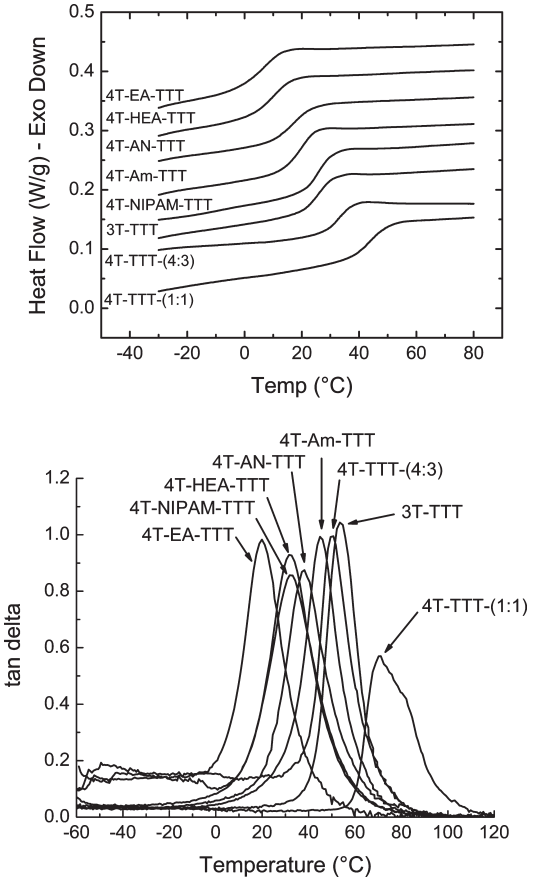

Figure 9. (a) DSC second heating scans and (b) tan δ vs temperature plots for modified thiol−ene films and controls.

DMTA-based glass transition temperatures (see Table 1) are higher. This results from the time-scale differences in DSC versus DMTA runs.

Simulated oxygen flux $J(t)$ curves generated for the networks (assuming 0.10 mm thick films) using their corresponding P and D values are shown in Figure 10 for comparison. The highest permeability was observed for the 4T-EA-TTT network with a value of 0.39 cm^3 (STP) cm m^{-2} day^{-1} atm^{-1}. As mentioned previously, this film is a relevant

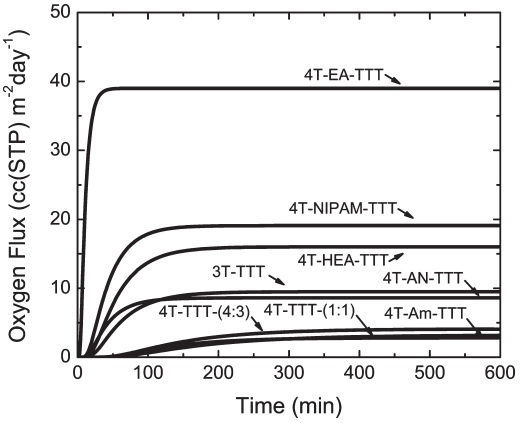

Figure 10. Simulated oxygen flux curves for modified thiol−enes and controls of 0.10 mm thickness.

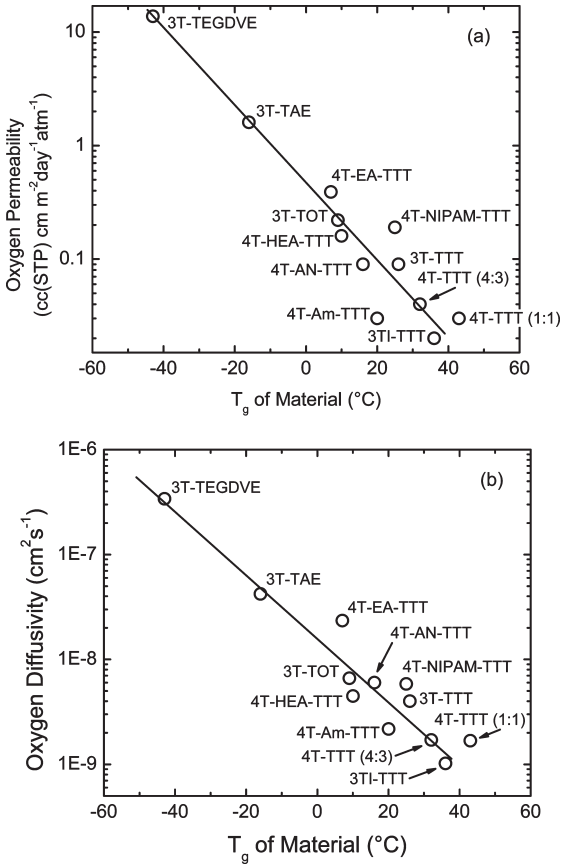

Figure 11. (a) Oxygen permeability vs T_g and (b) oxygen diffusivity vs T_g for modified and control thiol−enes.

control for the modified thiol−enes. The permeabilities of the other modified films are all lower, demonstrating the effect of strongly interacting functional groups in increasing oxygen barrier properties at room temperature. The oxygen solubility data exhibit in particular remarkable behavior: with the exception of the 4T-HEA and 4T-NIPAM systems, each of the modified films show solubilities lower than that of any of the other basic thiol−ene networks. Secondary interactive forces, dipole−dipole interactions from the cyano group of acrylonitrile, and hydrogen bonding from the amide group of acrylamide[22] hinder oxygen transport in the network.

Figure 11 shows semilog dependencies of oxygen permeability and diffusivity versus T_g for the modified films. The

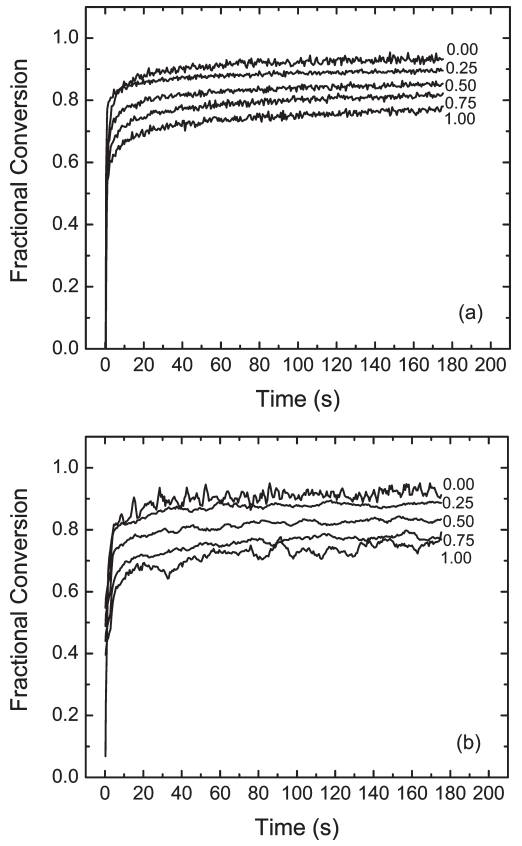

Figure 12. RT:FTIR group conversion versus time for 4T-Am:EA-TTT systems: (a) thiol conversion; (b) ene conversion. Labels denote acrylamide molar fraction in Michael reaction feed used to make the respective modified thiols.

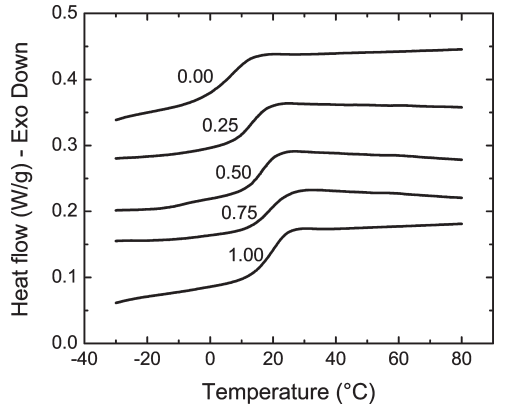

Figure 13. DSC second heating scans for series of 4T-Am:EA-TTT-modified thiol−ene films. Labels denote acrylamide molar fraction for Michael reaction feed used to make the respective trifunctional thiols.

corresponding values for the basic thiol−ene networks from Tables 1 and 2 are also added to this plot. As one may see, the data for all modified networks roughly followed the same trend as the family of basic networks showing noticeable variation.

As seen in Figure 11b, the thiol−ene films with accessible hydrogen-bonding species, 4T-HEA-TTT and 4T-Am-TTT, exhibited permeability and diffusivity values that fall below the corresponding trend established for the basic networks. This was attributed to the accessibility of the hydrogen-bonded functional groups in the modified networks implying improved cohesion and thus lower oxygen permeability and diffusivity.

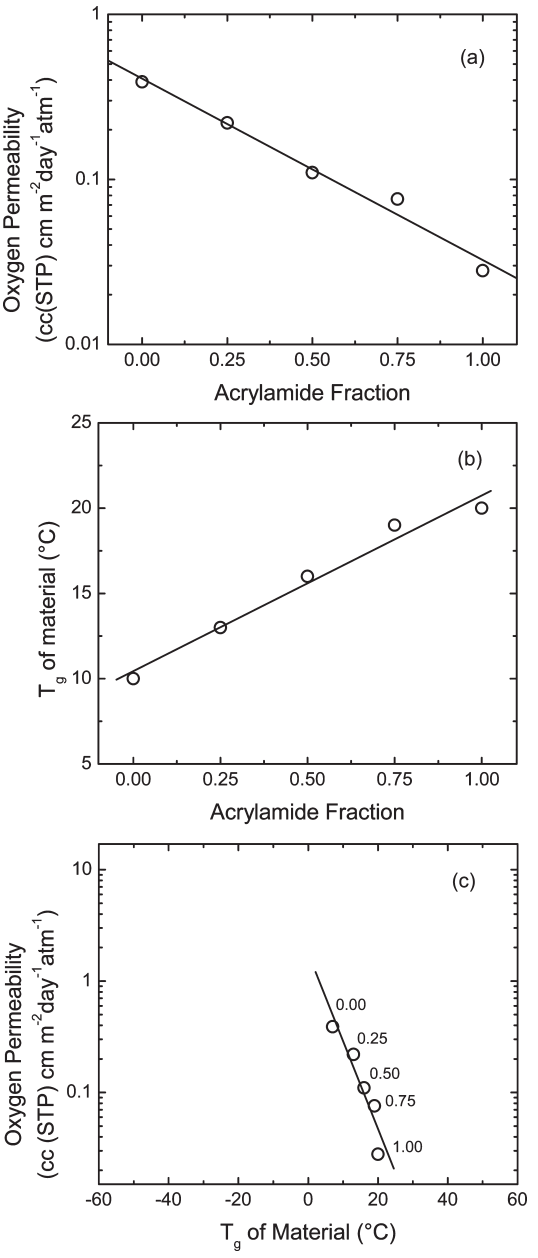

Figure 14. (a) Semilog plot of oxygen permeability and acrylamide fraction substituted onto thiol group of 4T, (b) linear plot of T_g and acrylamide fraction, and (c) semilog plot of oxygen permeability and T_g for the 4T-Am:EA-TTT networks.

To further evaluate the effect of the amide functional group on T_g and gas transport properties, a series of modified trifunctional thiol monomers were synthesized by using the thio-Michael addition of a combination of ethyl acrylate and acrylamide at different concentrations. An average of one out of every four groups on the 4T thiol monomer was capped by either an ethyl acrylate or acrylamide unit at varying relative concentrations: 0:100 (the pure ethyl acrylate 4T-EA), 25:75, 50:50, 75:25, and 100:0 (the pure acrylamide 4T-Am). Networks cured from these mixtures are referred to by the molar fraction of acrylamide in the Michael reaction feed: 0.00, 0.25, 0.50, 0.75, and 1.00. Real-time IR kinetics for both thiol and ene functional group conversion are shown in Figure 12. Both the thiol and ene conversion decreases as acrylamide fraction increases; the highest and lowest conversions were obtained by the pure 4T-EA-TTT and pure 4T-Am-TTT samples,

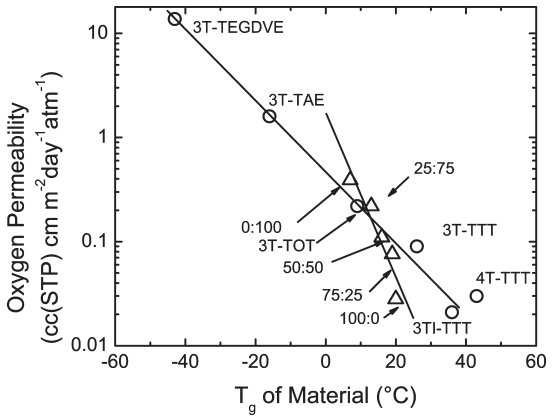

Figure 15. Relationship between oxygen permeability and the T_g of 4T-Am:EA-TTT-modified thiol−ene films compared to that of basic thiol−ene films.

respectively. It appears that an increase in hydrogen bonding of the amide group, derived from increased acrylamide fraction, lowers final conversion due to restriction in mobility of monomer species during polymerization. As previously discussed, the light intensity used to photocure films for glass transition and oxygen permeability measurements was much higher to ensure high conversions in all cases. According to Figure 13 which shows DSC second heating scans for fully cured films, the T_g (see Table 1) also increases as a function of increasing acrylamide content due to enhanced hydrogen bonding and resulting network mobility restrictions.

The oxygen transport results for the series of modified films given in Table 2 indicate a decrease in oxygen permeability with an increase in acrylamide molar fraction. Figure 14a shows that an increase of the acrylamide fraction results in an exponential decrease in oxygen permeability. This decrease is a direct consequence of restriction in mobility in the thiol−ene network due to hydrogen bonding. Interestingly, somewhat similar behavior was previously observed in the case of linear copolymers.[1] Exponential changes in permeability are established as a function of comonomer molar fraction leading to development of the Permachor concept.[1] Interestingly, thiol−ene network T_g also increases with increasing amide molar fraction but only linearly as shown in Figure 14b, thus resulting in an exponential decrease of oxygen permeability of acrylamide-modified networks with corresponding T_g, i.e., the difference between T_g and T_{test}.

It is important to notice that the plot in Figure 14c is similar to those in Figures 3 and 11, further illustrating the general correlation of log(P) and the difference between T_{test} and T_g for both the base thiol−ene networks (Figure 3), the modified thiol−ene networks (Figure 11), and the thiol−amide−ethyl−ene networks (Figure 14). However, the slope of the semilog plot in Figure 14c for the 4T-Am:EA-TTT-based networks is greater than that of the corresponding plots in Figures 3 and 11. This deviation can be seen in Figure 15 which includes all of the basic thiol−ene systems along with all of the 4T-Am:EA-TTT systems. Therefore, amide-modified thiol−ene networks form a different kind of family with regards to oxygen barrier properties versus T_g as compared to basic thiol−ene networks

Finally, annealing of selected films for 4 h at 100 °C in air was conducted to demonstrate that sufficient film curing was provided by the Fusion lamp in order to optimize conversion. Oxygen permeability values given in Table 2 for the annealed films are similar to oxygen permeability values for nonannealed films. This implies that the maximum of chemical conversion has been reached upon UV curing at room temperature leading to ultimate oxygen barrier properties, and no further postcuring is required.

Table 1. Glass Transition Temperatures Determined by DSC and DMTA

material	T_g (°C) (DSC)	T_g (°C) (tan δ peak)
3T-TEGDVE	−48	
3T-APE	−15	
3T-TOT	9	
3T-TTT	26	54
4T-TTT (1:1)	43	71
4T-TTT (4:3) (dangling thiol)	32	50
3TI-TTT	36	
4T-IPDI-TTT	65	
4T-EA-TTT	10	20
4T-AN-TTT	20	38
4T-HEA-TTT	16	32
4T-NIPAM-TTT	25	32
4T-Am-TTT	20	45
25:75 Am:EA	13	
50:50 Am:EA	16	
75:25 Am:EA	19	

Conclusions

The oxygen transport characteristics, specifically permeability, diffusivity, and solubility, were studied for a variety of thiol−ene networks. Using commercially available monomers, the functionality, rigidity, and type of ene group were varied, allowing the photopolymerization of networks spanning 100 °C in T_g. One network which showed high oxygen barrier properties was selected for further chemical modification. New thiol monomers were synthesized by a thio-Michael addition reaction of a tetrathiol to functionalized acrylates. These modified thiols were copolymerized with an isocyanurate-based ene monomer. The modified networks allowed an exploration into the effects of appendage groups with varied chemical structure (hydroxyl, amide, cyano, and alkyl) on T_g and oxygen barrier properties.

Both oxygen permeability and oxygen diffusivity, measured at room temperature, correlated remarkably well with T_g for both the rubbery and glassy networks, in agreement with classic behavior. Minimums in oxygen permeability, diffusivity, and solubility were found for samples whose glass transitions were near room temperature where the oxygen permeation measurements were conducted. Thus, V-shaped correlations of both permeability and diffusivity with T_g were drawn. These relationships can allow prediction of the room-temperature oxygen transport properties of any basic thiol−ene network simply by knowing its glass transition temperature.

Using the network modification platform, the T_g and oxygen barrier properties were tuned by changing the nature and concentration of the functional group in the network. Of particular interest was the introduction of primary amides as dangling appendages which resulted in especially low oxygen permeability. As the result of a hydrogen-bonding effect from the primary amide group, a deviation from the trend seen with basic thiol−enes was observed. The use of thiol−ene networks as a platform to investigate the systematic effect of functional groups on network properties has far-reaching implications. This method allows for the general assessment of how chemical structure can affect physical, mechanical, transport, and even optical properties of polymer networks.

Acknowledgment. The authors acknowledge Bruno Bock, Bayer Material Science, and Ciba Specialty Chemicals for materials and Fusion UV Systems for the light source.

References and Notes

(1) Salame, M. *Polym. Eng. Sci.* **1986**, *26*, 1543.
(2) Lee, W. M. *Polym. Eng. Sci.* **1980**, *20*, 65.
(3) Lang, J.; Wyser, Y. *Packag. Technol. Sci.* **2003**, *16*, 149.
(4) Sekelik, D. J.; Stepanov, E. V.; Nazarenko, S.; Schiraldi, D.; Hiltner, A.; Baer, E. *J. Polym. Sci., Part B: Polym. Phys.* **1999**, *37*, 847.
(5) White, J. E.; Haag, A. P.; Garth, P. R.; et al. *J. Polym. Sci., Part A: Polym. Chem.* **1996**, *34*, 2967.
(6) Brennan, D. J.; Silvis, H. C.; White, J. E.; Brown, C. N. *Macromolecules* **1995**, *28*, 6694.
(7) Kloosterboer, J. G. *Adv. Polym. Sci.* **1988**, *84*, 8.
(8) Kaya, E.; Smith, T.; Nayak, B.; Mathias, L. J. *Polym. Prepr.* (*Am. Chem. Soc., Div. Polym. Chem.*) **2005**, *46*, 857.
(9) Hoyle, C. E.; Lee, T. Y.; Roper, T. *J. Polym. Sci., Part A: Polym. Chem.* **2004**, *42*, 5301.
(10) Choi, J.; Lee, K. M.; Wycisk, R.; Pintauro, P. N.; Mather, P. T. *Macromolecules* **2008**, *41*, 4569.
(11) Hiltner, A.; Liu, R. Y. F.; Baer, E. *J. Polym. Sci., Part B: Polym. Phys.* **2005**, *43*, 1047.
(12) Crank, J. *The Mathematics of Diffusion*; Oxford University Press: New York, 1975.
(13) Pauly, S. Permeability and Diffusion Data. In *Polymer Handbook*; Brandrup, J., et al. Eds.; John Wiley & Sons: New York, 1999.
(14) Shin, J.; Nazarenko, S.; Hoyle, C. E. *Macromolecules* **2008**, *41*, 6741.
(15) Cook, W. D.; Chausson, S.; et al. *Polym. Int.* **2008**, *57*, 469.
(16) Cook, W. D.; Chen, F.; et al. *Polym. Int.* **2007**, *56*, 1572.
(17) Cohen, M. H.; Turnbull, D. *J. Chem. Phys.* **1959**, *31*, 1164.
(18) Yampol'skii, Y. P.; Volkov, V. V. *J. Membr. Sci.* **1991**, *64*, 191.
(19) Lin, H.; Freeman, B. D. *J. Mol. Struct.* **2005**, *739*, 57–74.
(20) Vrentas, J. S.; Duda, J. L. *J. Appl. Polym. Sci.* **1978**, *22*, 2325.
(21) Lee, T. Y.; Roper, T. M.; et al. *Macromolecules* **2004**, *37*, 3659.
(22) Galetich, I.; Stepanian, S. G.; et al. *J. Phys. Chem. A* **2000**, *39*, 104.